The Role of Ions on the Surface-Bound Water Structure at the Silica/Water Interface: Identifying the Spectral Signature of Stability†

Benjamin Rehl and Julianne M. Gibbs*

Department of Chemistry, University of Alberta, Edmonton, Alberta, T6G 2G2, Canada. julianne.gibbs@ualberta.ca

† Electronic supplementary information (ESI) available. Local field effect corrections of the SFG spectra, a brief maximum entropy method description, a comparison of nonresonant HD-SHG phase changes to known error phase changes, equations for calculating diffuse layer and surface nonlinear susceptibilities, a calculation of the electrostatic force acting on surface waters, and the analysis using calculated surface potentials.

TOC Graphic

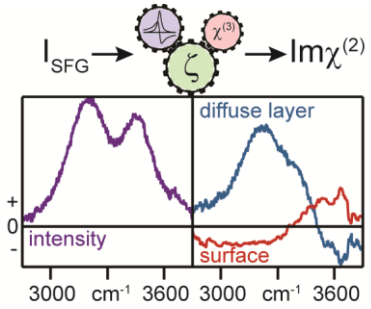

Abstract

We explore the influence of salt addition on the structure of water interacting closely with a charged silica surface. Isolating these surface effects is challenging, even with surface-specific techniques like sum frequency generation (SFG), because of the presence of aligned water nanometers to microns away from the charged silica. Here we combine zeta potential and SFG intensity measurements with the maximum entropy method and reported heterodyne second harmonic and sum frequency generation results to deconvolute from the total signal intensity the SFG spectral contributions of the waters adjacent to the surface. Deconvolution reveals that at very low ionic strength the surface water structure is similar to that of a neutral silica surface near the point of zero charge with waters oriented in opposite directions. This result suggests the known metastability of silica near the PZC and the stability of silica in low ionic strength solutions may originate from the same source, these oppositely oriented surface-bound waters. Orientation changes are induced upon adding salt, which lead to a decrease in the total amount of aligned water at the surface.

I. Introduction

The surface-bound water molecules that hydrate silica are believed to play a large role in the stability of silica in aqueous solutions despite consisting of only one or two monolayers of water.[1] Most notably, the stability of silica against aggregation in the absence of a net surface charge is highly unique, as most colloids are unstable near their point-of-zero charge (PZC).[1-2] This stability has been attributed to the interfacial water structure, but structural signatures of such stability have not yet been identified. Moreover, for silica this unusual stability is also observed at very low ionic strength near neutral pH, which lies well above the PZC (~pH 2), but quickly diminishes upon adding small quantities of ions.[1] In addition to ion influence on silica aggregation, ions are known to induce dissolution[3-4] and surface charging on silica,[5-8] as well as modulate the

electric double layer structure.[9-14] Yet, how these waters closely bound to the surface are affected by ions is unknown as they are difficult to measure by conventional spectroscopic techniques.

Vibrational sum frequency generation (SFG) spectroscopy is one technique that is well suited to study such buried interfaces owing to its selection rule that, within the electric dipole approximation, requires a break of inversion symmetry for SFG to occur. However, for charged surface/aqueous interfaces, traditional SFG fails to disentangle the response of the surface-bound waters from those aligned further away from the surface by the static electric field (i.e. within the diffuse layer).[15] Recent studies have suggested the contribution of the latter to the overall SFG spectrum can be significant depending on the surface charge density and the ionic strength.[16-19]

In 2016, it was shown by Wen et al. that the spectral behaviour of such surface waters, also called the bonded interfacial layer (BIL), at a Langmuir-Blodgett film could be separated from that stemming from the diffuse layer using a model that we refer to as the $\chi^{(3)}$ method.[18] One challenge with their experimental approach, however, was it required phase-sensitive SFG measurements that can be difficult to properly reference.[20-22] Furthermore, their analysis required knowledge of the surface potential, which the authors calculated from the surface charge density determined from the fitted SFG amplitudes of the negatively charged carboxylates with Gouy-Chapman theory. Similarly, recent SFG analyses[23-24] aimed at extracting information of the surface-bound waters from the silica/water interface at single pH values calculated surface potentials from dissociation constants estimated from earlier second harmonic generation[25-26] and chromatography studies.[27] Independently measuring the surface potential would be ideal as different surface preparations and samples for mineral oxides can influence the surface structure,[26, 28-30] but this is complicated by the insulating nature of silica.

These recent vibrational SFG experiments[24] as well as non-resonant heterodyne second harmonic generation (HD-SHG) experiments[31] proposed that the total surface water contributions of the silica/water interface changed upon adding salt at a constant pH. Tuladhar et al. has also shown that the OH vibrational lifetimes of the water at the surface vary considerably with salt concentration.[15] Yet these studies did not measure the spectral changes associated with the surface-bound waters. To determine how the hydrogen-bonding environment of these surface waters change with salt, here we utilize intensity rather than phase-sensitive SFG measurements coupled with streaming current measurements to determine the influence of salt addition on the surface-bound water, or BIL, structure at natural pH (CO_2 equilibrated ~pH 6). To obtain the phase information required to deconvolute the surface and diffuse layer responses, we use the maximum entropy method (MEM) with reference to two phase-sensitive SFG measurements of silica interfaces in the presence of neat water and 10 mM phosphate buffer[32] and several HD-SHG measurements over the ionic strength range explored in this work.[31] This analysis reveals that the hydrogen-bonded structure as well as the net alignment of the surface waters changes upon salt addition. Moreover, the water structure at very low salt concentration at pH 6 is similar to the reported structure at the PZC (pH 2),[32] where silica is also known to be stable,[1-2] suggesting that the signatures of silica stability are oppositely oriented surface water species. Our combined experimental approach coupled with MEM analysis offers significant advantages for deconvoluting the surface water response as it is less technically challenging than previous approaches yet more comprehensive owing to its reliance on separate types of measurements. As such, this work provides a general route to decipher the surface water structure under a variety of experimental conditions.

II. Experimental Methods

Materials. NaCl (99.99%, trace metals basis, Alfa Aesar) was used to prepare salt solutions and KCl (99.999%, trace metals basis, Acros Organics) was used to calibrate the SurPASS instrument. HPLC-grade MeOH (Fisher Chemical) was used for substrate cleaning. Sulfuric acid (95.0-98.0%, Caledon Laboratories) and hydrogen peroxide (30% w/w in H_2O, Sigma-Aldrich) were mixed in a 3:1 ratio and used for piranha cleaning substrates. All materials were used without further purification. Ultrapure deionized water (18.2 MΩ·cm) was used after deionization from a Milli-Q Direct 8 Water Purification System (Millipore, ZR0Q008WW). IR-grade fused quartz hemispheres (Almaz Optics, KI, 1 in. diameter) were used for SFG experiments. IR-grade fused quartz windows (Almaz Optics, KI, 2.5 in. diameter, 8 mm thickness) were used for zeta potential experiments. Sealing and spacer foils (Anton Paar, 97835 and 97834) were used to construct the flow channel along the fused quartz windows in the SurPASS clamping cell (Anton Paar, 22653).

Sample Preparation. Prior to an SFG experiment, an IR-grade fused quartz hemisphere was rinsed and sonicated (5 min) in ultrapure water, HPLC-grade MeOH, ultrapure water, and then ultrapure water again before being immersed in piranha solution (3:1 H_2SO_4:H_2O_2, 1 h). The hemisphere was then washed by the same water/MeOH rinse/sonication cycles as mentioned above followed by drying in an oven at 110°C (15 min) and then drying further in the atmosphere while covered in a clean, glass petri dish (15 min). A Teflon sample cell, built in-house and described elsewhere,[8] was rinsed and sonicated in ultrapure water, HPLC-grade MeOH, and ultrapure water again before being allowed to dry in open atmosphere. Prior to a zeta potential experiment, two IR-grade fused quartz windows were cleaned in the same way as described above. One window was modified in-house by drilling two holes through it, aligned to the specifications of the SurPASS clamping cell, to facilitate the measurement. The clamping cell insert (Anton Paar, 21411) was rinsed and sonicated in ultrapure water, HPLC-grade MeOH, and ultrapure water again

before being allowed to dry in open atmosphere. Onto the clean, dry clamping cell insert was placed a sealing foil. The clean, dry, modified fused quartz window was then placed on top of the sealing foil with the holes aligned. A spacer foil was then carefully placed on top of the window with the holes and channel aligned. Finally, a second fused quartz window was placed on top of the spacer foil to complete the channel. On top of the second fused quartz window was placed a support plate (Anton Paar, 84439) and the whole stack was placed within the clamping cell and tightened. A set of SurPASS Ag/AgCl electrodes (Anton Paar, 22667) were then connected through the clamping cell insert. Two concentrations of NaCl solution (10 mM and 1 M) were used to manually increase the sample solution ionic strength for SFG experiments. Solutions for zeta potential measurements were prepared by diluting 1 M NaCl solution. Solutions were prepared fresh and stored open to atmosphere for approximately 3 hours before data collection.

Caution: *Piranha solution is corrosive and explosive. Extreme heat is generated upon addition of hydrogen peroxide to sulfuric acid. Never add sulfuric acid to hydrogen peroxide, as hydrogen peroxide concentrations greater than 50% can be explosive. Piranha solution reacts violently with organics, and therefore organic solvents should not be stored nearby.*

Laser Assembly. A regeneratively amplified laser (Spectra-Physics, Spitfire Pro, 1 KHz, 94 fs, 3.3 W) was seeded and pumped, respectively by a Ti-sapphire oscillator (Spectra-Physics, MaiTai, 80 MHz) and a Nd:YLF laser (Spectra-Physics, Empower 30) to generate high peak power 800 nm pulses. This 800 nm was passed through a 35% beam splitter (Newport) directing 2.3 W to pump a noncollinear optical parametric amplifier (TOPAS-C/NDFG, Light Conversion) to produce a tunable, broadband IR light (FWHM = ~90 cm^{-1}). An infrared longpass filter (Edmund Optics, 2.40 μm, 68-653) was used to remove any residual signal and idler contribution from the IR beam, which was then passed through a polarizer (Thorlabs, LPMIR050-MP2), a zero-order,

tunable half-wave plate (Alphalas), and a CaF_2 focusing lens (Thorlabs, f = 500 mm) before reaching the sample. The remaining 1.0 W of 800 nm light from the Spitfire Pro was passed through an air-spaced Fabry-Perot Etalon (TecOptics) to generate narrow, picosecond pulses (FWHM = ~7 cm^{-1}). The visible light was then passed through a delay stage, a polarizer (Thorlabs LPVIS050-MP2), a zero-order, half-wave plate (Thorlabs, λ/2@808 nm), and a BK7 focusing lens (Thorlabs, f = 500 mm) before reaching the sample. The visible (~10-20 μJ/pulse) and IR (~18 μJ/pulse) beams were directed at the sample cell at incident angles of 61° and 67°, respectively, relative to the surface normal. The beams were slightly defocused to avoid beam-induced sample damage while spatially and temporally overlapped at the sample interface to generate sum frequency light. The SFG reflection beam was passed through a BK7 recollimating lens (Thorlabs, f = 400 mm), a half-wave plate (Thorlabs, λ/2@808 nm), a Glan-Thompson calcite polarizer (Thorlabs, GTH10M), a BK7 focusing lens (Thorlabs, f = 100 mm), and a filter (Thorlabs, FES0750) before entering a spectrograph (Princeton Instruments, Acton SP-2556 imaging spectrograph, grating: 600 grooves/mm, 500 nm blaze wavelength) connected to a thermoelectrically cooled (-75 °C), back-illuminated, charge-coupled device camera (Princeton Instruments, Acton PIXIS 100B CCD digital camera system, 1340 x 100 pixels, 20 um x 20 um pixel size).

SFG Experiments. A fused quartz hemisphere (Almaz Optics, KI, 1 in. diameter) with a gold-coated planar side (200 nm) was mounted to the clean sample cell. The laser was aligned and the SFG signal was optimized using the signal from the silica/gold interface. A nonresonant reference spectrum was collected at a single delay setting using eight IR pulses with centres ranging from ~2900-3600 cm^{-1}. A polystyrene calibration film (International Crystal Laboratories, 38 μm thick) was used to calibrate the detected frequency by comparison to three known

polystyrene aromatic C-H absorptions centered at 3026, 3059 and 3081 cm^{-1}. The gold-coated hemisphere was then exchanged for a freshly cleaned fused quartz hemisphere. The cell cavity was rinsed five times with ultrapure water and then allowed to equilibrate in ultrapure water for 30 minutes. NaCl solution was then added by micropipette to achieve the lowest ionic strength solution (0.01 mM) in the cell and allowed to equilibrate for 30 minutes. After acquisition, the ionic strength was further increased through the addition of concentrated NaCl by micropipette (Gilson, calibrated by Transcat, Inc.). Each subsequent solution was allowed to equilibrate with the fused quartz surface for 15 minutes before measurement. After collecting all sample spectra, the hemisphere was exchanged once more for the gold-coated hemisphere and a reference spectra was collected. Sample spectra were collected in ssp polarization (s-sum frequency, s-visible, p-infrared) for 120 s at each frequency used for the gold reference. Reference spectra were collected in ssp polarization for 1s per center frequency averaged over 10 acquisitions. All spectra were background corrected by subtraction with a background spectrum collected immediately prior to each sample or reference spectrum. Background spectra were collected by blocking the IR laser and acquiring signal at a single pulse. SFG intensities were normalized to the 3200 cm^{-1} intensity of the silica/water interface at 10 mM NaCl.

Zeta Potential Experiments. Zeta potential measurements were performed on a SurPASS Electrokinetic Analyzer (Anton Paar) using the clamping cell. The conductivity probe (Anton Paar, 18116) was calibrated prior to each experiment with 0.1 M KCl solution. Before setting up the clamping cell, the electrodes were connected by connection tube (Anton Paar, 100083) and the instrument was cleaned with ultrapure water four times (300 s for each cleaning cycle). After mounting the clamping cell to the instrument and connecting the electrodes, the instrument was filled with ultrapure water (200 s fill time) and a flow check was performed (500 mbar) to confirm

linear flow rate with respect to pressure. The cell was then rinsed with ultrapure water (500 mbar for 500 s) and allowed to equilibrate for 30 minutes. Higher ionic strength solutions were prepared, as described above, while the fused quartz window equilibrated under the current solution. Each solution was filled (200 s) into the instrument, followed by rinsing (500 mbar for 500 s) and equilibrated for at least 15 minutes before measurement, except for the initial introduction of NaCl which was allowed to equilibrate for at least 30 minutes. Measurements were performed under streaming current mode with a rinse target pressure of 500 mbar for 180 s and a ramp target pressure of 400 mbar for 20 s. The clean, calibrated conductivity probe was allowed to sit in the sample solution during the entire experiment.

Zeta potentials are calculated according to the following equation,[33]

$$\zeta = \frac{dI_{sc}}{d\Delta p} \times \frac{\eta}{\varepsilon \times \varepsilon_0} \times \frac{L}{A}, \quad \text{eq. 1}$$

where ζ is the zeta potential, I_{sc} is the streaming current, Δp is the change in pressure, η is the viscosity of the solution, ε is the relative permittivity of water, ε_0 is the vacuum permittivity, L is the length of the channel, and A is the area of the channel.

III. Results and Discussion

The $\chi^{(3)}$ method, originally proposed by Ong et al.,[25] and widely accepted by others,[16-17, 19, 31, 34-45] separates the total SFG signal at the silica/water interface in the OH stretching region into two origins: water assembled non-centrosymmetrically at the surface due to hydrogen bonding or ion hydration given by the second-order nonlinear susceptibility of the surface, $\chi_S^{(2)}$, and waters aligned or polarized by the static electric field emanating into the bulk from the charged surface

given by the product of the third-order nonlinear susceptibility, $\chi^{(3)}$, and the electrostatic potential Φ. This relationship is shown by the following equation

$$\sqrt{I_{SFG}} \propto E_{SFG} \propto \chi^{(2)}_{total} = \chi^{(2)}_{S} E_{Vis} E_{IR} + \chi^{(3)} E_{Vis} E_{IR} \int_0^\infty E_0(z) e^{i\Delta kz} dz, \quad \text{eq. 2}$$

where I_{SFG} is the SFG intensity, E_{Vis} and E_{IR} are the electric fields of the visible and infrared laser light sources incident on the silica surface, Δk is the wavevector mismatch of the sum frequency, visible, and infrared electric fields, E_{SFG} is the electric field of the sum frequency light generated at the interface, and $\chi^{(2)}_{total}$ is the total second order nonlinear susceptibility. The spectrum of $\chi^{(3)}$ is similar to that of bulk water,[19] which is consistent with the diffuse layer exhibiting bulk-like hydrogen bonding with a small amount of net alignment due to the presence of the static electric field. This static electric field emanating in the z-direction (along the surface normal) can be related to the electrostatic potential $\Phi(z)$ according to $E_0(z) = -\frac{d\Phi(z)}{dz}$.[46]

Although the potential at the silica surface is often invoked in the $\chi^{(3)}$ technique,[47-49] according to the Gouy-Chapman-Stern-Grahame model of the electric double layer, the potential which aligns water in the diffuse layer is that outside of the outer Helmholtz plane (OHP), rather than the surface. This diffuse layer potential, which we argue is the potential that contributes to the $\chi^{(3)}$ term, is often approximated as the zeta potential (ζ), which is experimentally determined based on the electrokinetic or electrophoretic properties of a system.[13-14] For the planar substrates we use for SFG measurements, the zeta potential can be measured in a flow set-up based on changes in streaming current or streaming potential with changes in applied pressure using the Helmholtz-Smoluchowski relationship. Therefore, we performed SFG measurements and streaming current measurements with the same type of silica and sample preparation to allow for a proper comparison between the resulting zeta potentials and the SFG response.

SFG intensity spectra were measured in the ssp-polarization combination (s-E_{SFG}, s- E_{vis}, p- E_{IR}) at natural pH (~pH 5.8 based on equilibration with atmospheric CO_2) with increasing salt concentration from pure water to 50 mM NaCl at the silica/aqueous interface as shown in Fig. 1. In the measured spectral window where the OH stretches of water and other species contribute, two large peaks and one smaller peak were observed, which we refer to as the 3200 cm^{-1}, 3400 cm^{-1}, and 3650 cm^{-1} modes, respectively. The first two modes are attributed to interfacial water while the latter has been assigned to isolated silanol groups[28] or to water experiencing a hydrophobic environment.[50] Consistent with earlier observations,[17, 24] the overall intensity of the SFG signal in this range increased with ionic strength until approximately 0.1 mM and then decreased with higher ionic strengths. This non-monotonic behaviour has been attributed to an interplay between the screening of the surface charges,[16, 51-54] and destructive signal interference within the diffuse layer.[17, 24, 36, 55-56] Above 0.1 mM the addition of salt led to a decrease in the integrated SFG intensity, which is qualitatively proportional to the amount of ordered water in the diffuse layer (Fig. 1b). As proposed by others,[17, 24] we attribute this drop to a decrease in the magnitude of the diffuse layer potential owing to increased charge screening by the cations, which is consistent with the decrease in zeta potential magnitude over the same range of salt concentrations (Fig. 1b). In contrast, below 0.1 mM the trend in SFG intensity deviated from the change in zeta potential magnitude. This difference below 0.1 mM ionic strength is attributed to waters aligned far away from the surface relative to the SF wavelength that generate signal out of phase from that produced closer to the surface. This difference in SF path length with salt results both in destructive interference and phase changes within the $\chi^{(3)}$ response[57-58] as quantified by the integral in equation 2 that relates not only to the interfacial potential but also to the z-dependence of the generated signal, which depends on the Debye length (hence ionic strength) as

well as the experimental geometry. The solution to this integral can be estimated for relatively low potentials below 25 mV as $\Phi_0\left[\frac{\kappa}{\kappa-i\Delta k_z}\right]$, or $\Phi_0 f_3$,[36] where Φ_0 is the surface potential, but for larger potentials like those measured here, the series expansion recently described by Hore and Tyrode is appropriate,[24]

$$\int_0^\infty E_0(z)e^{i\Delta kz}dz = \Phi_0 - \frac{4ik_bT\Delta k}{e}\sum_{n=1}^{\infty}\frac{\xi^{2n-1}}{(2n-1)(i\Delta k-\kappa(2n-1))} = g_3. \quad \text{eq. 3}$$

Here k_b, T, e, and κ are the Boltzmann constant, temperature, elementary charge, and inverse Debye length, respectively. ξ is a dimensionless parameter defined as $\tanh\left(\frac{e\Phi_0}{4k_bT}\right)$. However, in contrast to Hore and Tyrode, in equation 3 we define z = 0 at the onset of the diffuse layer, rather than the surface plane. This modification avoids including the surface water molecules that contribute to $\chi_S^{(2)}$ in the $\chi^{(3)}$ term based on the assumption that for resonant SFG, the orientation rather than the polarization of water plays a larger role in the $\chi^{(3)}$ response.[19] Although the surface potential might influence the surface water structure to some extent, hydrogen bonding is expected to dominate the orientation of water at the surface (see supporting information for calculation), which justifies defining the onset of the diffuse layer as the 0-plane for the $\chi^{(3)}$ response. Therefore to calculate g_3, the surface potentials of equation 3 are substituted by the zeta potentials, which provide an approximation of the diffuse layer potentials (Fig. 1b). The trend in calculated g_3 matches well with the square root of the integrated SFG intensity. This comparison indicates either that the diffuse layer waters are the dominant contributors to the SFG signal, or that the surface water structure is changing in such a way to yield the observed similarity between g_3 and the integrated intensity. However, as recent studies have shown,[24, 31, 59] the surface water structure

likely exhibits an ionic strength dependence, which cannot be ascertained from a comparison of g_3 and the integrated intensity.

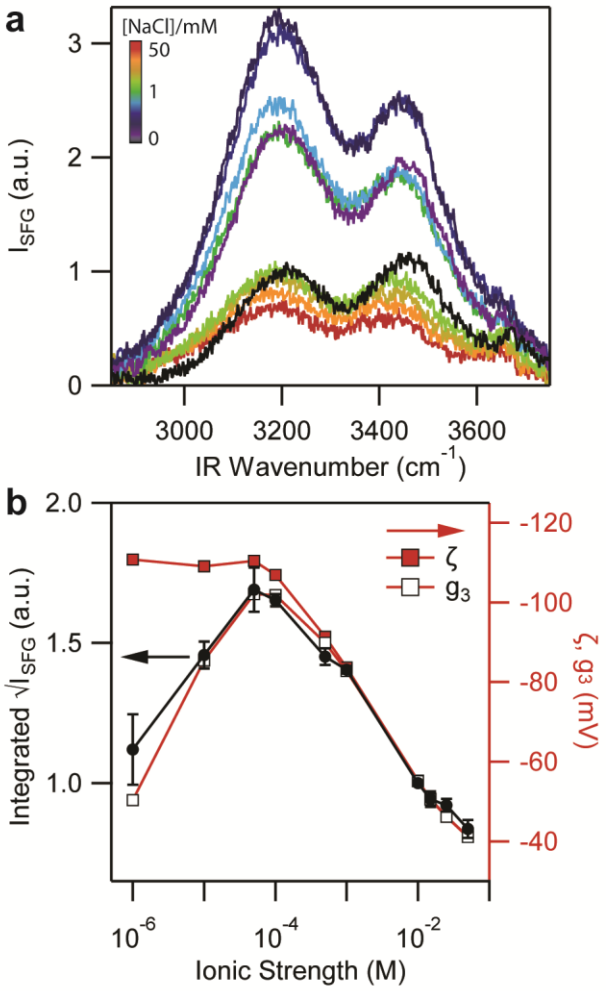

Fig. 1 (a) Representative SFG intensity corrected for local field effects from 2850 to 3750 cm^{-1} at the silica/water interface over an ionic strength range of pure water (black) to 50 mM NaCl (red). (b) The square root of the average integrated SFG intensity compared to the average ζ potentials and the corresponding g_3 values measured from the same type of silica under the same experimental conditions. The error bars are the standard deviation of three experiments for SFG measurements and two experiments for zeta potential measurements.

To deconvolute the $\chi_S^{(2)}$ and $\chi^{(3)}g_3$ responses and achieve a deeper understanding of these structural changes with salt addition, the phase of the SFG signal (i.e. the complex $\chi_{\text{total}}^{(2)}$ spectrum rather than the $\left|\chi_{\text{total}}^{(2)}\right|^2$ intensity spectrum) is required. To this end, SFG spectral analysis was performed with the maximum entropy method (MEM)[60-69] to predict the relative phase of the SF response at all frequencies by maximizing the spectral entropy and forbidding the growth of resonances over time.[70] However, because the MEM models an autoregressive process, there is an associated error spectrum of unknown phase.[61, 71] Therefore some *apriori* knowledge is required to determine this so-called error phase. For this information we were fortunate to consider the heterodyne SFG measurements of the silica/water interface from Myalitsin et al.[32] Specifically, since the error phase can be modeled as a linear equation following a frequency squeezing procedure,[60] the resonant phase measurement of the silica/neat water interface by Myalitsin et al.[32] was used to determine the error phase slope and intercept of our silica/pure water spectrum (Fig. 2a and 2b). Despite the different experimental geometries, which could affect the measured lineshape,[24] the resulting complex spectrum determined from the MEM analysis of our intensity spectrum at the silica/pure water interface with this error phase agrees well with that measured using phase-sensitive SFG by Myalitsin et al. (Fig. 2b).[32]

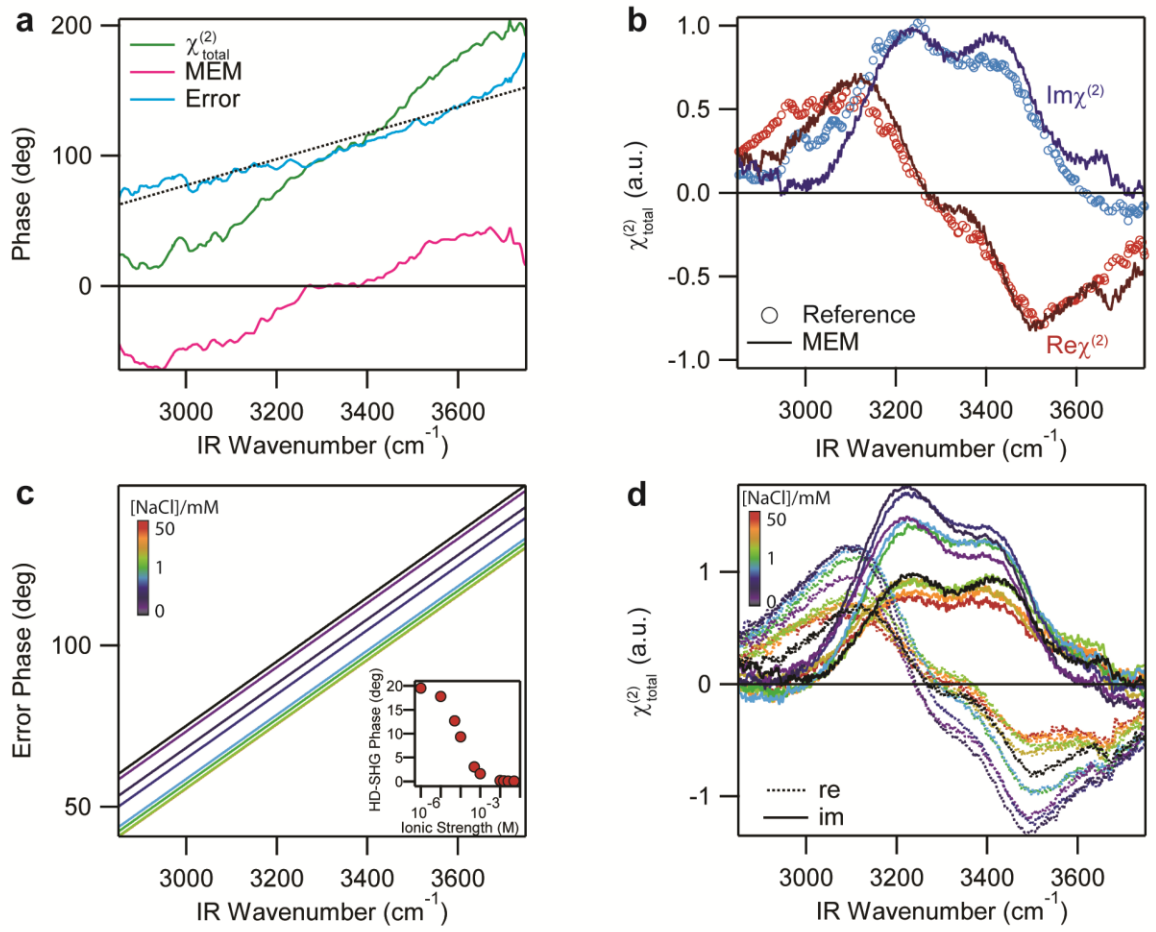

Fig. 2 (a) $\chi^{(2)}_{\text{total}}$ phase of the silica/neat water interface measured by Myalitsin et al.,[32] and maximum entropy and error phases calculated from the corresponding $\left|\chi^{(2)}_{\text{total}}\right|^2$ using the MEM. The dashed black line is a linear fit to the error phase. (b) Complex spectrum predicted by the MEM from the measured SFG intensity of the silica/pure water interface (lines) by referencing the complex spectrum of the silica/neat water interface (circles) from Myalitsin et al.[32] (c) Error phases used for the MEM from pure water to 50 mM NaCl calculated using linear equations of identical slope offset by the HD-SHG nonresonant phases measured by Ohno et al. and fit to a sigmoid to extract values at the desired ionic strengths (inset).[31] (d) Complex spectra predicted by the MEM from measured SFG intensities of the silica/water interface from pure water (black) to 50 mM

NaCl (red) using the HD-SFG phase of silica/neat water interface[32] and the HD-SHG phases of the silica/$NaCl_{(aq)}$ interface[31] as reference.

Comparison of the phase derived from the MEM to an experimentally measured phase from heterodyne SFG yields the error phase for a single spectrum. However, since such heterodyne SFG measurements are not available over the ionic strength range of interest, we must estimate how the error phase changes with salt addition. Since the MEM predicts the relative phase of all contributing modes but not the absolute phase with respect to the origin, we require knowledge of how the error phase changes with increasing salt concentration. We propose the salt dependence of the relative error phase in our system stems from the change in phase of the $\chi^{(3)}$ (or diffuse layer) response based on the relative change between the Debye and coherence lengths with changing salt concentration. This phase change of the diffuse layer signal can be calculated by g_3, allowing the error phase to be compensated accordingly. However, the magnitude of this compensation depends not just on the relative amplitude phase and g_3 but the magnitude of all modes contributing to $\chi_S^{(2)}$ and $\chi^{(3)}$.[72] As we do not know the relative magnitude of $\chi_S^{(2)}$ and $\chi^{(3)}$ in our system, the solution is underdetermined. Heterodyne SHG has been used to measure the phase and amplitude of the net non-resonant signal under similar experimental conditions of increasing salt concentration at the natural pH of ~6. The salt dependence of the HD-SHG phase was proposed to stem from the change in phase of the $\chi^{(3)}$ (or diffuse layer) response based on the relative change of the Debye and coherence lengths with changing salt concentration.[31] Yet, using the change in signal phase of the HD-SHG as an estimate of the change in error phase in our MEM analysis assumes that the signals measured by HD-SHG and SFG originate from the same source. For vibrational SFG in our experimental window, the signal is modulated primarily by the net orientation and number density of water molecules. For nonresonant SHG, the water are also

expected to dominate the signal although other oscillators such as the silica may also contribute.[45] Moreover, the magnitude ratio of $\chi_S^{(2)}$ and $\chi^{(3)}$ would have to be the same on and off resonance for the signal phase angle to be identical in both experiments. Nevertheless, the change in HD-SHG signal phase is intrinsically related to the change in the diffuse layer thickness, which should play a significant role in the resonant SFG spectra as well.

To determine whether the change in measured HD-SHG phase can be used to approximate the change in error phase, we performed MEM analysis on the silica/10 mM phosphate buffer interface (pH 6.7) where the complex spectrum was also known from phase-sensitive SFG[32] after reconstructing the corresponding real spectra (see supporting information). By comparing the measured phase and the MEM phase, the error phase magnitude was calculated and compared with that determined for the silica/neat water interface. The change in error phase between these two spectra was ~20°, which is consistent with the HD-SHG phase change between that measured for the silica/neat water and silica/10 mM NaCl interface (18°). This agreement in the error phase change and the HD-SHG signal phase change suggests that HD-SHG can be used to predict how the error phase changes in vibrational SFG experiments with MEM analysis. Therefore MEM analysis was performed on our SFG intensity spectra using the error phase determined from the phase-sensitive SFG reference of pure water offset by the change in phase measured by HD-SHG (Fig. 2c). The resulting complex SFG spectra are shown in Fig. 2d.

For the imaginary spectra, $\mathrm{Im}\chi_{\mathrm{total}}^{(2)}$, the 3200 and 3400 cm^{-1} modes remained positive over the entire ionic strength range (Fig. 2d), which we propose stems from a net orientation of water with hydrogens pointed towards the surface at all salt concentrations due primarily to the negative surface and the expected alignment of the water dipoles with the corresponding static electric field. Similarly the mode at 3650 cm^{-1} that has been assigned to either surface silanol sites[28] or water

molecules in a hydrophobic environment[50] did not change orientation with added salt. However, in the low wavenumber range below 3100 cm^{-1}, a small negative feature grew in and receded with increasing salt concentration. The identity of this low wavenumber mode is unclear, but it has been proposed to be water molecules which are H-bond acceptors with the surface silanols and oriented with their oxygens towards the surface.[73]

We also present the real spectra as a function of salt concentration, as identifying the pH where it crosses through zero is useful for comparing our complex spectra to those reported by other groups (Fig. 2d). Interestingly, we observed that the wavenumber where the real spectra passed through zero blue shifted with increasing ionic strength. This blue shift in the zero-point crossing with increasing salt may help to understand the differences between the complex spectrum measured by Myalitsin et al. of the fused silica/neat water interface,[32] and the complex spectra measured by Ostroverkhov et al. of the α-quartz/water interface, as the pH cycling performed in the latter to make the surface more amorphous likely increased the solution ionic strength.[73] Our reconstructed real spectrum from the imaginary and square magnitude spectra of the silica/10 mM phosphate buffer interface reported by Myalitsin et al. also exhibits this blue shifted zero-point crossing relative to that of neat water consistent with salt leading to a blue shift (Fig. S2).

With the complex spectra and g_3 in hand, we next needed the relative magnitude of $\chi^{(3)}$, which should remain constant under the conditions of this study.[74] To find $\chi^{(3)}$ we required a particular ionic strength range where $\chi_S^{(2)}$ was unchanging. Then the corresponding $\chi_{\text{total}}^{(2)}$ difference spectrum calculated from equations 2 and 3 should equal the reported $\chi^{(3)}$ spectrum[18] after accounting for the change in diffuse layer potential and interference determined by the g_3 term. By taking the difference of the complex $\chi_{\text{total}}^{(2)}$ for spectra measured at adjacent salt

concentrations, we found the difference spectrum between 0.1 mM and 0.5 mM consistently yielded, with respect to replicated experiments, a similar $\chi^{(3)}$ as that reported by Wen et al. (see supporting information).[18] This finding supports the recent work of Hore and Tyrode, which predicted the integrated $\chi_S^{(2)}$ from 2800-3800 cm^{-1} to be relatively unchanging around this ionic strength range.[24] To account for variation in the actual zeta potential between the sum frequency spectra replicates, we report the average $\chi^{(3)}$ from three independently collected sets of spectra analyzed using the average zeta potential values from duplicate streaming current experiments (Fig. 3a). The resulting $\chi^{(3)}$ spectrum is largely negative in the imaginary domain except for a small positive mode above 3600 cm^{-1}. Interestingly, this positive feature, which was also present in the diffuse layer spectra calculated at the silica/H_2O and the silica/HOD interfaces by Urashima et al.,[23] indicates that some OH groups of bulk-like water are oriented in opposition to the static electric field.

With the $\chi^{(3)}$ spectrum determined, the diffuse layer spectra at all ionic strengths can be readily calculated by taking the product of the $\chi^{(3)}$ spectrum and the corresponding g_3 value (Fig. 3b). These resulting diffuse layer spectra, which have incorporated the effect of interference calculated by g_3, exhibit the same non-monotonic trend as the SFG intensities. The imaginary diffuse layer spectra are dominated by two positive modes around 3200 cm^{-1} and 3400 cm^{-1} with a small negative feature at higher wavenumbers. The change in lineshape of the diffuse layer spectra with changing salt concentration is due to the dependence of the g_3 term on the wavelength, ionic strength, and diffuse layer potential.[24] The result of these dependences reveals an increasingly negative and red shifting contribution at high wavenumber with decreasing ionic strength, which we note is not due to structural changes to the diffuse layer, but rather highlights how interference within the diffuse layer can alter the apparent lineshape measured at the detector.[57-58] Interestingly,

the lineshapes of our diffuse layer spectra where interference plays less of a role between 1 mM and 50 mM NaCl agree well with that reported by Urashima et al. at high pH (pH 12) and similar salt concentrations (0.01 to 0.1 M).[23]

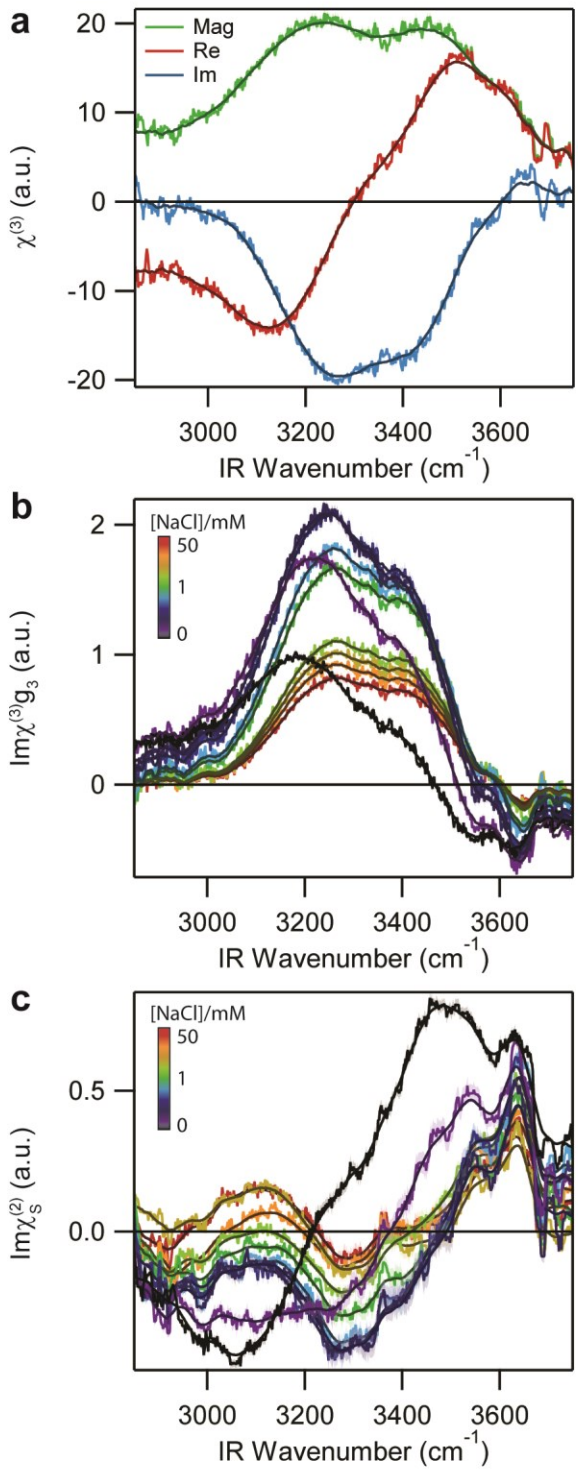

Fig. 3 (a) The complex spectrum of the third order nonlinear susceptibility determined from the total complex difference spectra between 0.1 mM and 0.5 mM NaCl divided by the difference in

the corresponding average g_3 values. The reported complex $\chi^{(3)}$ spectrum is the average from analysing three SFG data sets. (b) The imaginary $\chi^{(3)}g_3$ spectra corresponding to the diffuse layer water contribution from the silica/aqueous interface from pure water (black) to 50 mM (red) ionic strength. (c) The imaginary $\chi_S^{(2)}$ spectra of the surface-bound waters for a representative data set from pure water (black) to 50 mM (red) ionic strength. Shaded regions in figures (a)-(c) are the uncertainty propagated from the standard deviation in measured ζ potentials. The bold lines represent the smoothed spectra.

The surface contributions as a function of salt concentration were then extracted from the total complex spectra by subtracting the corresponding diffuse layer spectra (Fig. 3c). In the resulting $\chi_S^{(2)}$ imaginary spectra we observed several features of opposite orientation across the entire spectral window, which suggested the presence of oppositely oriented water populations hydrogen bonded at the surface. Importantly, the presence of these oppositely oriented water molecules is largely absent in the total complex spectrum, which is dominated by the diffuse layer contribution. In general, the $\chi_S^{(2)}$ imaginary spectra from pure water to 50 mM NaCl exhibited negative features at lower wavenumber and positive features at higher wavenumber. Specifically, for the pure water imaginary $\chi_S^{(2)}$ spectrum, a negative mode around 3050 cm^{-1} and positive modes around 3250, 3450, and 3630 cm^{-1} were observed. With salt addition, the positive modes around 3250 and 3450 cm^{-1} decreased in magnitude until ~0.05 mM NaCl. This decrease of the high wavenumber mode is consistent with a recent MD simulation that observed an under-coordinated water population at the neutral silica/water interface that disappeared upon salt addition.<ref> At higher salt concentrations, the imaginary spectrum from 2850 – 3450 cm^{-1} is entirely negative. Simultaneously the positive peak around 3630 cm^{-1} decreased in magnitude from its value in pure

water until ~0.05 mM NaCl was reached. With further salt addition, the positive high wavenumber modes remained relatively constant while a positive feature grew in around 3100 cm^{-1}.

Notably, the $\mathrm{Im}\chi_S^{(2)}$ spectra at low ionic strength (≤0.01 mM) and pH 6 are similar to the imaginary spectra of the silica/H_2O and silica/HOD interfaces measured by Myalitsin et al.[32] near the point of zero charge (~pH 2), as well as the calculated spectrum from MD simulations of the neutral surface.[19] At pH 2, the spectrum should be dominated by the surface response owing to the lack of an interfacial potential aligning the diffuse layer. The SFG spectra derived from MD simulations of an uncharged, hydrophobic silica/water interface also exhibited these two modes of opposite phase originating from waters close to the surface.[75] The similarity in surface water structure at low ionic strength, where the silica has a negative zeta potential ($\zeta \approx$ -110 mV), and the neutral silica surface at pH 2 is not obvious from a direct comparison of the intensity spectra owing to the significance of the $\chi^{(3)}g_3$ contribution to the total complex spectra for the former. One possibility is this similarity between the $\mathrm{Im}\chi_S^{(2)}$ spectra at pH 6 below 0.01 mM NaCl and the reported[32] imaginary spectra at pH 2 stems from similarities in the surface charge densities under the two conditions as silica is expected to have very little surface charge at very low ionic strength (requiring near neutral pH). If the Stern layer is absent at low ionic strength, then the surface charge density is approximately equal in magnitude and opposite in sign to the charge density of the diffuse layer (i.e. $\sigma_0 \approx -\sigma_{DL}$).[76] With our measured zeta potential at the lowest salt concentration explored (0.01 mM NaCl at ~pH 6), we calculated from the Grahame equation a σ_0 of -0.79 mC/m^2, which is significantly smaller than the value calculated at 50 mM (-21 mC/m^2) from the corresponding zeta potential. This suggests a very low percentage of deprotonated silanols in nearly pure water (0.1% deprotonated for a silanol density of 4.6 per nm^2)[1] suggesting a similar density of silanol groups as would be present near the point-of-zero charge (~pH 2). Accordingly

we reason the similar surface hydrogen-bonding water structure under these two conditions stems from the similar silanol density. As previously mentioned, the stability of silica colloids against aggregation in the presence of ions is significant at pH 2 but drops as the pH is raised until near neutral values.[1-2] However near neutral pH in the absence of any additional salt, silica colloids also exhibit this stability, which quickly diminishes with salt addition.[1] We propose that the opposite orientation of waters at the surface is a spectral signature of this enhanced stability.

Previous phase-sensitive measurements by Myalitsin et al. at the silica/water interface assigned the water populations based on their resonant frequency and the sign of $\mathrm{Im}\chi^{(2)}_{total}$.[32] Using these assignments as a starting point, we assign the positive peaks from 3250 - 3450 cm^{-1} in the pure water/silica imaginary $\chi^{(2)}_S$ spectrum to waters which donate H-bonds to silanols, and the negative peak around 3050 cm^{-1} to waters which accept H-bonds from silanols. Our assignment is supported by the phase measurements of Ostroverkhov et al. at the α-quartz/water interface at pH 1.5, to which the low and high frequency modes were attributed to waters with their hydrogens pointed away and towards the surface, respectively.[73] Furthermore, our assignments are also consistent with MD simulations and DFT calculations of a neutral α-quartz/water interface by Joutsuka et al. that yielded a negative low wavenumber band and a positive high wavenumber band in the imaginary spectra originating from waters accepting H-bonds from and donating H-bonds to silanols, respectively.[19] The subsequent decrease in magnitude of the large negative feature with increasing salt concentrations is consistent with increasing surface charge density, corresponding with a decrease in the number of silanols and H-bond acceptor waters (Fig. 4). As the surface charge density becomes more negative with increasing salt concentration, the positive feature around 3100 cm^{-1} grows in. Therefore we assign this positive 3100 cm^{-1} mode to the waters which donate a hydrogen bond to the charged siloxides in agreement with the work of Urashima

et al.[23] Additionally, the trends in imaginary surface spectra evolution with increasing surface charge density are consistent with recent MD simulations of hydrophobic and hydrophilic silica in contact with water.[75] In those simulations, the calculated imaginary nonlinear susceptibility was negative at low wavenumber and positive at high wavenumber for a hydrophobic silica surface. The opposite signs at both low and high wavenumber were observed for the hydrophilic surface. Therefore, we propose that the silica transitions from hydrophobic at low salt and low surface charge density to hydrophilic at higher salt and higher surface charge density based on the change in the Im$\chi_S^{(2)}$ spectra. However, a recent time-resolved SFG/MD-DFT study suggested the opposite near the PZC based on the change in water coordination observed in the simulations.[15] Finally, the positive feature around 3630 cm^{-1} may originate from either H-bonded isolated silanols[28] or waters dangling over hydrophobic sites such as siloxanes, which do not reorient with the addition of salt.[50] We note in the former case, the silanols would be net oriented with their OH groups pointed below the surface plane given the sign of Im$\chi_S^{(2)}$.

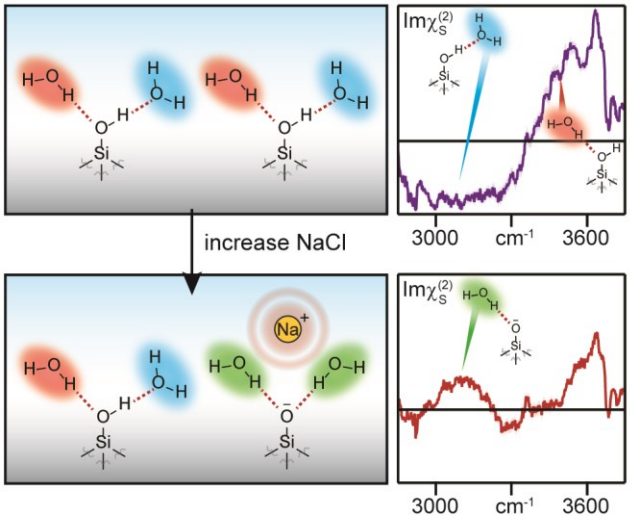

Fig. 4 Proposed arrangement of surface waters hydrogen bonded to silica under lower (top) and higher (bottom) salt concentrations and the corresponding Im$\chi_S^{(2)}$ spectral features.

IV. Conclusions

In summary, we determined the effect of ionic strength on the SFG spectra of the surface-bound waters at the silica/water interface through deconvolution of the spectra into surface-bound water, or $\chi_S^{(2)}$, and diffuse layer water, or $\chi^{(3)}g_3$, components. In lieu of a calculated surface potential for the analysis, we obtained the zeta potential from streaming current measurements, which has been related to both SFG[77-78] and SHG,[79-81] but not used to deconvolute the $\chi_S^{(2)}$and $\chi^{(3)}$ contributions. With the reported phase-sensitive SFG[32] and SHG[31] measurements of the silica/water interface as reference, we applied the maximum entropy method to our measured SFG intensities to obtain the complex SFG spectra. These complex spectra and the measured ζ potentials were used to determine the $\chi^{(3)}$ spectrum at the silica/water interface, which agrees well with that of Wen et al.[18] We then extracted the surface-bound water $\chi_S^{(2)}$ imaginary spectra with increasing salt concentration near the natural pH of 6 and observed significant changes over this ionic strength range. In particular, we observed a change in sign in the low wavenumber mode with increasing salt concentration, indicative of an orientation change of water that contributes at these wavenumbers. We note that recent reports analyzing the $\chi_S^{(2)}$ and $\chi^{(3)}$ contributions based on non-resonant SHG and integrated SFG intensities have also proposed that $\chi_S^{(2)}$ is highly salt dependent.[24, 31] Yet our work here establishes how both the $\chi_S^{(2)}$ and $\chi^{(3)}g_3$ imaginary spectra change with salt addition, providing molecular insight. Specifically, the similarity of our $\chi_S^{(2)}$ spectra at low salt concentrations to the total complex spectrum near the PZC[32] suggests the signature of stability at the silica/water interface is oppositely oriented surface waters.

Conflicts of interest

There are no conflicts of interest to declare.

Author Information

Corresponding Author:

*E-mail: julianne.gibbs@ualberta.ca

ORCID

Benjamin Rehl: 0000-0002-5534-6717

Julianne M. Gibbs: 0000-0001-5819-2306

Acknowledgements

J.M.G. gratefully acknowledges the Natural Sciences and Engineering Research Council of Canada for an Accelerator Award, the Alfred P. Sloan Foundation for a Research Fellowship, and Petro-Canada for a Young Innovator Award. B.R. gratefully acknowledges support from the Alberta/Technical University of Munich International Graduate School for Hybrid Functional Materials (ATUMS-NSERC CREATE) program, the Natural Sciences and Engineering Research Council of Canada for a Canadian Graduate Scholarship, and the Queen Elizabeth II Graduate Scholarship. We thank Prof. Dennis Hore (University of Victoria), Prof. Franz Geiger (Northwestern University), Prof. Sean Roberts (University of Texas), and Shyam Parshotam (University of Alberta) for insightful discussions.

References

1. Iler, R. K., *The Chemistry of Silica: Solubility, Polymerization, Colloid and Surface Properties, and Biochemistry*. New York: Wiley: 1979.
2. Lyklema, J., *Fundamentals of Interface and Colloid Science: Particulate Colloids*. Elsevier: 2005; Vol. 4.

3. Karlsson, M.; Craven, C.; Dove, P. M.; Casey, W. H., Surface Charge Concentrations on Silica in Different 1.0 M Metal-Chloride Background Electrolytes and Implications for Dissolution Rates. *Aquat. Geochem.* **2001,** *7* (1), 13-32.
4. Icenhower, J. P.; Dove, P. M., The Dissolution Kinetics of Amorphous Silica into Sodium Chloride Solutions: Effects of Temperature and Ionic Strength. *Geochim. Cosmochim. Ac.* **2000,** *64* (24), 4193-4203.
5. Salis, A.; Parsons, D. F.; Boström, M.; Medda, L.; Barse, B.; Ninham, B. W.; Monduzzi, M., Ion Specific Surface Charge Density of SBA-15 Mesoporous Silica. *Langmuir* **2010,** *26* (4), 2484-2490.
6. Dove, P. M.; Craven, C. M., Surface Charge Density on Silica in Alkali and Alkaline Earth Chloride Electrolyte Solutions. *Geochim. Cosmochim. Ac.* **2005,** *69* (21), 4963-4970.
7. Kitamura, A.; Fujiwara, K.; Yamamoto, T.; Nishikawa, S.; Moriyama, H., Analysis of Adsorption Behavior of Cations onto Quartz Surface by Electrical Double-layer Model. *J. Nucl. Sci. Technol.* **1999,** *36* (12), 1167-1175.
8. Azam, M. S.; Weeraman, C. N.; Gibbs-Davis, J. M., Specific Cation Effects on the Bimodal Acid-Base Behavior of the Silica/Water Interface. *J. Phys. Chem. Lett.* **2012,** *3*, 1269-1274.
9. Behrens, S. H.; Grier, D. G., The Charge of Glass and Silica Surfaces. *J. Chem. Phys.* **2001,** *115* (14), 6716-6721.
10. Jalil, A. H.; Pyell, U., Quantification of Zeta-Potential and Electrokinetic Surface Charge Density for Colloidal Silica Nanoparticles Dependent on Type and Concentration of the Counterion: Probing the Outer Helmholtz Plane. *J. Phys. Chem. C* **2018,** *122* (8), 4437-4453.
11. Kosmulski, M., Positive Electrokinetic Charge of Silica in the Presence of Chlorides. *J. Colloid Interf. Sci.* **1998,** *208* (2), 543-545.
12. Franks, G. V., Zeta Potentials and Yield Stresses of Silica Suspensions in Concentrated Monovalent Electrolytes: Isoelectric Point Shift and Additional Attraction. *J. Colloid Interf. Sci.* **2002,** *249* (1), 44-51.
13. Brown, M. A.; Goel, A.; Abbas, Z., Effect of Electrolyte Concentration on the Stern Layer Thickness at a Charged Interface. *Angew. Chem. Int. Ed.* **2016,** *55*, 3790 - 3794.
14. Brown, M. A.; Abbas, Z.; Kleibert, A.; Green, R. G.; Goel, A.; May, S.; Squires, T. M., Determination of Surface Potential and Electrical Double-Layer Structure at the Aqueous Electrolyte-Nanoparticle Interface. *Phys. Rev. X* **2016,** *6* (1), 011007.
15. Tuladhar, A.; Dewan, S.; Pezzotti, S.; Brigiano, F. S.; Creazzo, F.; Gaigeot, M.-P.; Borguet, E., Ions Tune Interfacial Water Structure and Modulate Hydrophobic Interactions at Silica Surfaces. *J. Am. Chem. Soc.* **2020,** *142* (15), 6991-7000.
16. Jena, K. C.; Covert, P. A.; Hore, D. K., The Effect of Salt on the Water Structure at a Charged Solid Surface: Differentiating Second- and Third-order Nonlinear Contributions. *J. Phys. Chem. Lett.* **2011,** *2*, 1056-1061.
17. Schaefer, J.; Gonella, G.; Bonn, M.; Backus, E. H. G., Surface-Specific Vibrational Spectroscopy of the Water/Silica Interface: Screening and Interference. *Phys. Chem. Chem. Phys.* **2017,** *19* (25), 16875-16880.
18. Wen, Y.-C.; Zha, S.; Liu, X.; Yang, S.; Guo, P.; Shi, G.; Fang, H.; Shen, Y. R.; Tian, C., Unveiling Microscopic Structures of Charged Water Interfaces by Surface-Specific Vibrational Spectroscopy. *Phys. Rev. Lett.* **2016,** *116* (1), 016101.
19. Joutsuka, T.; Hirano, T.; Sprik, M.; Morita, A., Effects of Third-Order Susceptibility in Sum Frequency Generation Spectra: A Molecular Dynamics Study in Liquid Water. *Phys. Chem. Chem. Phys.* **2018,** *20* (5), 3040-3053.
20. Xu, X.; Shen, Y. R.; Tian, C., Phase-Sensitive Sum Frequency Vibrational Spectroscopic Study of Air/Water Interfaces: H_2O, D_2O, and Diluted Isotopic Mixtures. *J. Chem. Phys.* **2019,** *150* (14), 144701.
21. Ahmed, M.; Nojima, Y.; Nihonyanagi, S.; Yamaguchi, S.; Tahara, T., Comment on “Phase-Sensitive Sum Frequency Vibrational Spectroscopic Study Of Air/Water Interfaces: H_2O, D_2O, and Diluted Isotopic Mixtures” [J. Chem. Phys. 150, 144701 (2019)]. *J. Chem. Phys.* **2020,** *152* (23), 237101.

22. Xu, X.; Shen, Y. R.; Tian, C., Response to "Comment on 'Phase-Sensitive Sum Frequency Vibrational Spectroscopic Study of Air/Water Interfaces: H_2O, D_2O, and Diluted Isotopic Mixtures'" [J. Chem. Phys. 152, 237101 (2020)]. *J. Chem. Phys.* **2020,** *152* (23), 237102.
23. Urashima, S.-h.; Myalitsin, A.; Nihonyanagi, S.; Tahara, T., The Topmost Water Structure at a Charged Silica/Aqueous Interface Revealed by Heterodyne-Detected Vibrational Sum Frequency Generation Spectroscopy. *J. Phys. Chem. Lett.* **2018,** *9* (14), 4109-4114.
24. Hore, D. K.; Tyrode, E., Probing Charged Aqueous Interfaces Near Critical Angles: Effect of Varying Coherence Length. *J. Phys. Chem. C* **2019,** *123* (27), 16911-16920.
25. Ong, S.; Zhao, X.; Eisenthal, K. B., Polarization of Water Molecules at a Charged Interface: Second Harmonic Studies of the Silica/Water Interface. *Chem. Phys. Lett.* **1992,** *191*, 327-335.
26. Darlington, A. M.; Gibbs-Davis, J. M., Bimodal or Trimodal? The Influence of Starting pH on Site Identity and Distribution at the Low Salt Aqueous/Silica Interface. *J. Phys. Chem. C* **2015,** *119* (29), 16560-16567.
27. Méndez, A.; Bosch, E.; Rosés, M.; Neue, U. D., Comparison of the Acidity of Residual Silanol Groups in Several Liquid Chromatography Columns. *J. Chromatogr. A* **2003,** *986* (1), 33-44.
28. Dalstein, L.; Potapova, E.; Tyrode, E., The Elusive Silica/Water Interface: Isolated Silanols Under Water as Revealed by Vibrational Sum Frequency Spectroscopy. *Phys. Chem. Chem. Phys.* **2017,** *19*, 10343-10349.
29. Sheth, N.; Ngo, D.; Banerjee, J.; Zhou, Y.; Pantano, C. G.; Kim, S. H., Probing Hydrogen-Bonding Interactions of Water Molecules Adsorbed on Silica, Sodium Calcium Silicate, and Calcium Aluminosilicate Glasses. *J. Phys. Chem. C* **2018,** *122* (31), 17792-17801.
30. Li, I.; Bandara, J.; Shultz, M. J., Time Evolution Studies of the H_2O/Quartz Interface Using Sum Frequency Generation, Atomic Force Microscopy, and Molecular Dynamics. *Langmuir* **2004,** *20* (24), 10474-10480.
31. Ohno, P. E.; Chang, H.; Spencer, A. P.; Liu, Y.; Boamah, M. D.; Wang, H.-f.; Geiger, F. M., Beyond the Gouy–Chapman Model with Heterodyne-Detected Second Harmonic Generation. *J. Phys. Chem. Lett.* **2019,** *10* (10), 2328-2334.
32. Myalitsin, A.; Urashima, S.; Nihonyanagi, S.; Yamaguchi, S.; Tahara, T., Water Structure at the Buried Silica/Aqueous Interface Studied by Heterodyne-Detected Vibrational Sum-Frequency Generation. *J. Phys. Chem. C* **2016,** *120* (17), 9357-9363.
33. Luxbacher, T.; Anton Paar Gmb, H., *The Zeta Potential for Solid Surface Analysis : A Practical Guide to Streaming Potential Measurement*. Anton Paar GmbH: Austria, 2014.
34. Gragson, D. E.; McCarty, B. M.; Richmond, G. L., Ordering of Interfacial Water Molecules at the Charged Air/Water Interface Observed by Vibrational Sum Frequency Generation. *J. Am. Chem. Soc.* **1997,** *119* (26), 6144-6152.
35. de Beer, A. G. F.; Campen, R. K.; Roke, S., Separating Surface Structure and Surface Charge with Second-Harmonic and Sum-Frequency Scattering. *Phys. Rev. B* **2010,** *82* (23), 235431.
36. Gonella, G.; Lütgebaucks, C.; de Beer, A. G. F.; Roke, S., Second Harmonic and Sum-Frequency Generation from Aqueous Interfaces Is Modulated by Interference. *J. Phys. Chem. C* **2016,** *120* (17), 9165-9173.
37. Dreier, L. B.; Bernhard, C.; Gonella, G.; Backus, E. H. G.; Bonn, M., Surface Potential of a Planar Charged Lipid–Water Interface. What Do Vibrating Plate Methods, Second Harmonic and Sum Frequency Measure? *J. Phys. Chem. Lett.* **2018,** *9* (19), 5685-5691.
38. Pezzotti, S.; Galimberti, D. R.; Shen, Y. R.; Gaigeot, M.-P., Structural Definition of the BIL and DL: A New Universal methodology to Rationalize Non-Linear $\chi^{(2)}(\omega)$ SFG Signals at Charged Interfaces, Including $\chi^{(3)}(\omega)$ Contributions. *Phys. Chem. Chem. Phys.* **2018,** *20* (7), 5190-5199.
39. Wang, H.; Xu, Q.; Liu, Z.; Tang, Y.; Wei, G.; Shen, Y. R.; Liu, W.-T., Gate-Controlled Sum-Frequency Vibrational Spectroscopy for Probing Charged Oxide/Water Interfaces. *J. Phys. Chem. Lett.* **2019**.

40. Boamah, M. D.; Ohno, P. E.; Lozier, E.; Van Ardenne, J.; Geiger, F. M., Specifics about Specific Ion Adsorption from Heterodyne-Detected Second Harmonic Generation. *J. Phys. Chem. B* **2019,** *123* (27), 5848-5856.
41. Chang, H.; Ohno, P. E.; Liu, Y.; Lozier, E. H.; Dalchand, N.; Geiger, F. M., Direct Measurement of Charge Reversal on Lipid Bilayers Using Heterodyne-Detected Second Harmonic Generation Spectroscopy. *J. Phys. Chem. B* **2020,** *124* (4), 641-649.
42. Lütgebaucks, C.; Gonella, G.; Roke, S., Optical Label-Free and Model-Free Probe of the Surface Potential of Nanoscale and Microscopic Objects in Aqueous Solution. *Phys. Rev. B* **2016,** *94* (19), 195410.
43. Didier, M. E. P.; Tarun, O. B.; Jourdain, P.; Magistretti, P.; Roke, S., Membrane Water for Probing Neuronal Membrane Potentials and Ionic Fluxes at the Single Cell Level. *Nat. Commun.* **2018,** *9* (1), 5287.
44. Bischoff, M.; Biriukov, D.; Předota, M.; Roke, S.; Marchioro, A., Surface Potential and Interfacial Water Order at the Amorphous TiO2 Nanoparticle/Aqueous Interface. *J. Phys. Chem. C* **2020,** *124* (20), 10961-10974.
45. Rehl, B.; Rashwan, M.; DeWalt-Kerian, E. L.; Jarisz, T. A.; Darlington, A. M.; Hore, D. K.; Gibbs, J. M., New Insights into χ(3) Measurements: Comparing Nonresonant Second Harmonic Generation and Resonant Sum Frequency Generation at the Silica/Aqueous Electrolyte Interface. *J. Phys. Chem. C* **2019,** *123* (17), 10991-11000.
46. Dalchand, N.; Cui, Q.; Geiger, F. M., Electrostatics, Hydrogen Bonding, and Molecular Structure at Polycation and Peptide:Lipid Membrane Interfaces. *ACS Appl. Mater. Inter.* **2019**.
47. Geiger, F. M., Second Harmonic Generation, Sum Frequency Generation, and $\chi^{(3)}$: Dissecting Environmental Interfaces with a Nonlinear Optical Swiss Army Knife. *Annu. Rev. Phys. Chem.* **2009,** *60*, 61-83.
48. Covert, P. A.; Hore, D. K., Geochemical Insight from Nonlinear Optical Studies of Mineral–Water Interfaces. *Annu. Rev. Phys. Chem.* **2016,** *67* (1), 233-257.
49. Backus, E.; Schaefer, J.; Bonn, M., The Mineral/Water Interface Probed with Nonlinear Optical Spectroscopy. *Angew. Chem. Int. Ed.* **2020**, 10.1002/anie.202003085.
50. Cyran, J. D.; Donovan, M. A.; Vollmer, D.; Siro Brigiano, F.; Pezzotti, S.; Galimberti, D. R.; Gaigeot, M.-P.; Bonn, M.; Backus, E. H. G., Molecular Hydrophobicity at a Macroscopically Hydrophilic Surface. *P. Natl. Acad. Sci. USA* **2019,** *116* (5), 1520.
51. Jena, K. C.; Hore, D. K., Variation of Ionic Strength Reveals the Interfacial Water Structure at a Charged Mineral Surface. *J. Phys. Chem. C* **2009,** *113*, 15364-15372.
52. Covert, P. A.; Jena, K. C.; Hore, D. K., Throwing Salt into the Mix: Altering Interfacial Water Structure by Electrolyte Addition. *J. Phys. Chem. Lett.* **2014,** *5*, 143-148.
53. Dewan, S.; Yeganeh, M. S.; Borguet, E., Experimental Correlation Between Interfacial Water Structure and Mineral Reactivity. *J. Phys. Chem. Lett.* **2013,** *4*, 1977-1982.
54. Yang, Z.; Li, Q.; Chou, K. C., Structures of Water Molecules at the Interfaces of Aqueous Salt Solutions and Silica:Cation Effects. *J. Phys. Chem. C* **2009,** *113*, 8201-8205.
55. Achtyl, J. L.; Vlassiouk, I. V.; Fulvio, P. F.; Mahurin, S. M.; Dai, S.; Geiger, F. M., Free Energy Relationships in the Electrical Double Layer over Single-Layer Graphene. *J. Am. Chem. Soc.* **2013,** *135* (3), 979-981.
56. Ohno, P. E.; Saslow, S. A.; Wang, H.-f.; Geiger, F. M.; Eisenthal, K. B., Phase-Referenced Nonlinear Spectroscopy of the α-Quartz/Water Interface. *Nat. Commun.* **2016,** *7*, 13587.
57. Ohno, P. E.; Wang, H.-f.; Geiger, F. M., Second-Order Spectral Lineshapes from Charged Interfaces. *Nat. Commun.* **2017,** *8* (1), 1032.
58. Ohno, P. E.; Wang, H.-f.; Paesani, F.; Skinner, J. L.; Geiger, F. M., Second-Order Vibrational Lineshapes from the Air/Water Interface. *J. Phys. Chem. A* **2018,** *122* (18), 4457-4464.

59. Marchioro, A.; Bischoff, M.; Lütgebaucks, C.; Biriukov, D.; Předota, M.; Roke, S., Surface Characterization of Colloidal Silica Nanoparticles by Second Harmonic Scattering: Quantifying the Surface Potential and Interfacial Water Order. *J. Phys. Chem. C* **2019,** *123* (33), 20393-20404.
60. Yang, P.-K.; Huang, J. Y., Phase-Retrieval Problems in Infrared–Visible Sum-Frequency Generation Spectroscopy by the Maximum-Entropy Method. *J. Opt. Soc. Am. B* **1997,** *14* (10), 2443-2448.
61. Yang, P.-K.; Huang, J. Y., Model-Independent Maximum-Entropy Method for the Analysis of Sum-Frequency Vibrational Spectroscopy. *J. Opt. Soc. Am. B* **2000,** *17* (7), 1216-1222.
62. Sovago, M.; Vartiainen, E.; Bonn, M., Determining Absolute Molecular Orientation at Interfaces: A Phase Retrieval Approach for Sum Frequency Generation Spectroscopy. *J. Phys. Chem. C* **2009,** *113* (15), 6100-6106.
63. Sovago, M.; Vartiainen, E.; Bonn, M., Observation of Buried Water Molecules in Phospholipid Membranes by Surface Sum-Frequency Generation Spectroscopy. *J. Chem. Phys.* **2009,** *131* (16), 161107.
64. de Beer, A. G. F.; Samson, J.-S.; Hua, W.; Huang, Z.; Chen, X.; Allen, H. C.; Roke, S., Direct Comparison of Phase-Sensitive Vibrational Sum Frequency Generation with Maximum Entropy Method: Case Study of Water. *J. Chem. Phys.* **2011,** *135* (22), 224701.
65. de Beer, A. G. F.; Chen, Y.; Scheu, R.; Conboy, J. C.; Roke, S., Analysis of Complex Spectra Using Fourier Filtering. *J. Phys. Chem. C* **2013,** *117* (50), 26582-26587.
66. Roy, S.; Covert, P. A.; Jarisz, T. A.; Chan, C.; Hore, D. K., Surface–Bulk Vibrational Correlation Spectroscopy. *Anal. Chem.* **2016,** *88* (9), 4682-4691.
67. Yang, W.-C.; Hore, D. K., Broadband Models and Their Consequences on Line Shape Analysis in Vibrational Sum-Frequency Spectroscopy. *J. Chem. Phys.* **2018,** *149* (17), 174703.
68. Johansson, P. K.; Koelsch, P., Vibrational Sum-Frequency Scattering for Detailed Studies of Collagen Fibers in Aqueous Environments. *J. Am. Chem. Soc.* **2014,** *136* (39), 13598-13601.
69. Hofmann, M. J.; Koelsch, P., Retrieval of Complex χ(2) Parts for Quantitative Analysis of Sum-Frequency Generation Intensity Spectra. *J. Chem. Phys.* **2015,** *143* (13), 134112.
70. Burg, J. P. Maximum Entropy Spectral Analysis Ph.D. Thesis, Stanford University, USA, Stanford, 1975.
71. Bos, A. v. d., Alternative Interpretation of Maximum Entropy Spectral Analysis. *IEEE T. Inform. Theory* **1971,** *17* (4), 493-494.
72. Rehl, B.; Gibbs, J. M., **Manuscript in Preparation**.
73. Ostroverkhov, V.; Waychunas, G. A.; Shen, Y. R., New Information on Water Interfacial Structure Revealed by Phase-Sensitive Surface Spectroscopy. *Phys. Rev. Lett.* **2005,** *94* (4), 046102.
74. Joutsuka, T.; Morita, A., Electrolyte and Temperature Effects on Third-Order Susceptibility in Sum-Frequency Generation Spectroscopy of Aqueous Salt Solutions. *J. Phys. Chem. C* **2018,** *122* (21), 11407-11413.
75. Smirnov, K. S., Structure and Sum-Frequency Generation Spectra of Water on Uncharged Q4 Silica Surfaces: A Molecular Dynamics Study. *Phys. Chem. Chem. Phys.* **2020,** *22* (4), 2033-2045.
76. Lyklema, J., *Solid-Liquid Interfaces*. Academic Press: San Diego, 1995; Vol. II.
77. Han, H.; Peng, M.; Hu, Y.; Nguyen, A. V.; Sun, W., An SFG Spectroscopy Study of the Interfacial Water Structure and the Adsorption of Sodium Silicate at the Fluorite and Silica Surfaces. *Miner. Eng.* **2019,** *138*, 178-187.
78. Rashwan, M.; Rehl, B.; Sthoer, A.; Darlington, A. M.; Azam, M. S.; Zeng, H.; Liu, Q.; Tyrode, E.; Gibbs, J. M., Structure of the Silica/Divalent Electrolyte Interface: Molecular Insight into Charge Inversion with Increasing pH. *J. Phys. Chem. C* **Just Accepted**.
79. Lützenkirchen, J.; Scharnweber, T.; Ho, T.; Striolo, A.; Sulpizi, M.; Abdelmonem, A., A Set-Up for Simultaneous Measurement of Second Harmonic Generation and Streaming Potential and Some Test Applications. *J. Colloid Interf. Sci.* **2018,** *529*, 294-305.

80. Kumal, R. R.; Karam, T. E.; Haber, L. H., Determination of the Surface Charge Density of Colloidal Gold Nanoparticles Using Second Harmonic Generation. *J. Phys. Chem. C* **2015,** *119* (28), 16200-16207.
81. Gan, W.; Wu, W.; Yang, F.; Hu, D.; Fang, H.; Lan, Z.; Yuan, Q., The Behavior of Hydroxide and Hydronium Ions at the Hexadecane–Water Interface Studied with Second Harmonic Generation and Zeta Potential Measurements. *Soft Matter* **2017,** *13* (43), 7962-7968.